An FEM-aided investigation of the deformation during Single Point Incremental Forming

S. He[1], A. Van Bael[1], P. Van Houtte[1], Y. Tunckol[2], J. Duflou[2], A.M.Habraken[3]

[1] Department of Metallurgy and Materials Engineering, Katholieke Universiteit Leuven, Kasteelpark Arenberg 44, B-3001 Leuven, Belgium

[2] Department of Mechanical Engineering, Katholieke Universiteit Leuven, Celestijnenlaan 300B, B-3001 Leuven, Belgium

[3] Department of Mechanics of Solids and Materials, Université de Liège, Chemin des Chevreuils 1, B-4000 Liege, Belgium

Abstract. Incremental forming is an innovative and flexible sheet metal forming technology for small batch production and prototyping, which does not require any dedicated die or punch to form a complex shape. This paper investigates the process of single point incremental forming of an aluminium cone both experimentally and numerically. Finite element models are established to simulate the process. The output of the simulation is given in terms of final geometry, the thickness profile of the product and the strain history and distribution during the deformation. Comparison between the simulation results and the experimental data is made.

Keywords: Finite element method, Incremental forming, Sheet metal

1. Introduction

The incremental sheet forming process has emerged in the past few years as a potential alternative to conventional sheet metal stamping processes. The process uses a smooth ended tool under numerical control to create a local indentation in a clamped sheet, and by dragging the point of contact around the sheet, according to a programmed tool path, a wide variety of shapes may be formed without the need for specific tooling. The goal of this technology is to meet the increasing need to produce prototypes and small batch productions at low cost. The advantage of the incremental forming approach is that it does not require any specialised tooling, and therefore offers flexibility with short setup times. Two versions of the process have been explored: with and without a supporting post on the reverse side of the workpiece. This paper will focus on the latter approach, so-called 'single point' incremental forming (SPIF).

Up to now most research efforts in the field of SPIF have been focused on the industrial applicability of the process and relevant advantages were demonstrated [1-4]. Various shapes have been achieved using different materials, which enlarges the potential applications of SPIF technology. In the mean time, some experimental research work has also been carried out to investigate the deformation mechanism and material behavior during SPIF [5-7]. Apart from experimental studies, numerical methods have also been applied to analyze the deformation process and influence of various process parameters [8-13]. However, this process is still in an early stage of development and requires much more research to better understand the deformation mechanism. This paper investigates incremental forming of an aluminium cone using the powerful tool of finite element (FE) analysis, with special emphasis on the evolution of global shape, sheet thickness distribution and the evolution of plastic strain.

2. Experimental Setup

A three-axis CNC vertical milling machine is used as the platform for the SPIF process. A cylindrical stylus with a 12.7mm diameter spherical head is placed in the mill spindle. As shown in figure 1, a 1.2mm thick blank sheet with dimensions of 225x225 mm is supported on a four-sided steel fixture and clamped rigidly to this fixture with a backing plate containing a 182mm diameter orifice. The backing plate is used to ensure a clear change of angle when the forming process is initiated at the sheet surface. A cone with an internal diameter of 180mm will be formed inside the orifice and truncated at a 40mm depth. During the process, the tool travels at a feed rate of 2000mm/min along a series of circular contours generated transverse to the radial direction of the cone, as shown in figure 2. After traveling the entire path of one contour, the tool moves deeper in a stepwise fashion to follow the next contour. This process is repeated until the desired depth is reached. The proportions of the step are controlled by both the vertical step size from one contour to the next and also the wall angle Φ of the cone. In the current study, the vertical step size was chosen as 0.5mm and cones with different wall angles of 50, 60 and 65 degrees were investigated. Anti-

wear hydraulic oil with a viscosity grade of 46 was used as lubricant between the tool and the blank. The material used is aluminium alloy AA3003 that was fully annealed after cold rolling.

After the cones were made, the geometry of the deformed cones was measured by a laser scanner, from which the shape of the cross sections as well as the thickness distribution of the cone was determined. The accuracy of the laser scanner is ±15 micron.

3. Finite Element Modeling

A three-dimensional, elasto-plastic FE model is set up for the simulation of the SPIF process. The FE package Abaqus/Standard is used in this work [14]. During the SPIF process, due to the localised deformation around the tool, there is no real symmetry and a model for the whole geometry should be established. Unfortunately such a simulation is very computationally demanding. Therefore, in the present study, axisymmetric boundary conditions are assumed for the blank during the process and a 40-degree pie of the blank is considered in the simplified model. Figure 3 shows the utilized FE model for the process. The rolling direction coincides with a symmetry axis, which is the 0-degree section of the meshed blank. A symmetry is also assigned to the 40-degree section so that the nodes on that section can only stay in that plane. As a result, the angle of the pie will remain unchanged during the simulation. Brick elements (element type C3D6 and C3D8R in the terminology of Abaqus) are utilized for the blank. The mesh consists of three layers of elements through the thickness and 2640 elements in each layer. Both the tool and the backing plate are modeled as rigid surfaces. Coulomb's friction law is applied with a friction coefficient of 0.05 describing the friction between the blank and the tool and 0.15 between the blank and the backing plate. The flow stress curve of the material obtained by tensile tests is approximated by the Swift law $\sigma=180(\varepsilon+0.00109)^{0.21}$ (MPa). Anisotropy of the material is not taken into account in the current model and the isotropic von Mises yield criterion is adopted.

During the simulation, the results of the 20-degree central section of the meshed blank are taken for further analysis to avoid any end effect due to the use of the partial model.

4. Results and Discussions

4.1. Geometry of Formed Cones

The geometric accuracy of the formed part is a major concern for the SPIF process. There are two possible sources for the errors concerning the geometry. Firstly, the tool path is generated exclusively according to the geometric information specified by the CAD model of the desired part, where the elastic portion of the deformation is neglected. As a consequence, the springback of the material could introduce some misfit. Secondly, since there is no proper die supporting the sheet during the forming process, the material has more freedom to deform, which makes it difficult to achieve the desired part, especially for complex shapes. Instead of the trial-and-error method, the FE modeling could be very helpful to improve the tool path design in order to obtain the target geometry.

In the present study, the simulated final geometry of the cones is compared with experimental results. Figure 4 shows the inner surfaces of the cones with 50, 60 and 65-degree wall angle. It is clear that the simulated shapes agree well with the experimental ones in the cone wall region for all cones. For the cone bottom, the simulated surfaces are deeper than the experimental ones with a maximum error of about 1.5mm at the center. This difference is probably due to the simplified FE model, in which only one part of the geometry is considered and the imposed boundary conditions do not represent the real interaction from neighbouring material. He et al. [12] have reported that a full model in which the whole blank is meshed without any assigned boundary conditions along the radial edges provides better results for the cone bottom. It is worth pointing out that elastic springback after the unloading does exist, especially in the cone bottom. For example, for the 50-degree cone, the center of the bottom moves up by 0.5mm when the tool is lifted from the blank. This springback should be taken into account during the tool path design.

4.2. Thickness profile

For conventional SPIF, it is known that the final thickness of the formed part strongly depends on the wall angle using tool paths as described in figure 2. Presuming volume constancy and a deformation mode close to plane strain condition occurring during the process, the actual thickness of the cone wall θ_1 for an initial thickness θ_0 and a given wall angle ϕ (figure 2) can be derived by the so-called sine law:

$$q_1 = q_0 \sin(90 - f) \tag{1}$$

The sine law, which is originally used in the spinning process [15], assumes a uniform wall thinning. This is true when the cone wall angle is relatively low. As the wall angle increases, a non-uniform thinning however takes place, resulting in localised thinning in the cone wall region.

Figure 5 illustrates the predicted and measured sheet thickness for the formed cones with different wall angles. Firstly, it can be seen that for all cones a quite good agreement with a maximum difference of less than 0.05mm is reached between the experimental and simulation results. Secondly, the thickness in the central region of the bottom of the cone remains unchanged, whereas the thickness in the wall region is reduced drastically. Thirdly, the thickness profile changes when the wall angle is different. For instance, for the 50-degree cone, the simulated thickness in the wall region is reduced from 1.2mm to 0.76mm being very close to the sine law value of 0.77mm, and almost uniform thinning takes place. With an increase of the wall angle, a localised thinning starts to occur on top of the normal thickness reduction, resulting in a non-uniform wall thinning. As shown in the figure, when the cone wall angle reaches 60 degrees, the simulated minimum thickness is about 0.54mm which is nearly 10% thinner than 0.60mm according to the sine law. The difference between the actual minimum thickness and the sine law value increases further to 16% for a wall angle of 65 degrees. A similar phenomenon is also observed experimentally for a 70-degree cone for a similar aluminium sheet [16]. However, despite of the localised thinning, the sine law is still satisfied for the stationary wall thickness level as shown in the figure. Furthermore, the localised thinning always takes place at a depth between 12 to 15mm in case of cone forming. It is

believed that this is the most critical area during the process. With the increase of the wall angle, the localised thinning becomes more and more severe, and finally leads to unexpected failure at a certain wall angle. Experimental work has demonstrated that a wall angle of 70 to 71 degrees can be considered as the maximum for the SPIF process for the used material with a thickness of 1.2mm. When the initial sheet thickness increases, the maximum wall angle that can be achieved without the occurrence of fracture also increases. For example, experimental observations show that the maximum wall angle can reach 75 degrees for an initial thickness of 2.0mm for the same aluminium alloy. An alternative in case of steep wall angle could be to use a two- pass or multiple pass strategy to avoid the excessive thinning and achieve the final geometry [3,17]. This is not explored further in this paper.

4.3. Strain History and Distribution

During the SPIF process, the deformation takes place locally as the tool moves contour by contour. During one contour, only the material close to the contact area with the tool undergoes limited deformation due to the small vertical step size. This small deformation accumulates over a series of subsequent contours. For a cone with a certain wall angle, the strain depends on the position of the material point on the sheet. In the present study, the plastic strain evolution is analyzed for the four elements in the inner surface layer of the cone indicated in figure 3. During the simulation, these four elements are subsequently affected by the movement of the tool: Element 1 (E1), which is close to the blank outer edge, is the first element to undergo deformation. But the final strain only reaches a limited level since it undergoes the tool action only during the first few contours. On the contrary, Element 4 (E4), which is close to the center of the blank, is not affected by the tool during the initial contours and the deformation takes place later in the process. As a result, the deformation there only reaches a limited level before the process finishes. Elements 2 (E2) and 3 (E3), lying in between, undergo the tool action for the maximum number of contours and consequently the strains also reach the maximum value there. This phenomenon is synthesized in figure 6, which shows the evolution of the accumulated equivalent plastic strain of the mentioned elements for a cone with a 50-degree wall angle.

As mentioned by Ambrogio et al. [11], the strain paths are characterized by a typical step-trend: each strain increment is the direct consequence of the action of the tool as it passes a particular element. In turn, no strain increment occurs when the tool continues its path along the same contour far away from that element. This confirms the feature of localised deformation that characterizes the SPIF process: a given material point undergoes its strain through progressive, small increments each time the tool passes by. Figure 7 shows the evolution of the normal plastic strain components of Element 3 in a local coordinate system having the local z-axis perpendicular to the blank surface and the local x-axis parallel to the cone radial direction along the wall surface. Figure 8 illustrates such a local coordinate system at a material point. This local coordinate system co-rotates with the cone wall during the simulation. As shown in figure 7, the radial, circumferential and thickness strain component correspond to the strain in the x, y and z direction respectively in the local coordinate system. Although the absolute values of all three components increase stepwise during

the process, it is noticed that the circumferential strain remains close to zero, which confirms that the simplified plane strain assumption for an axisymmetric SPIF process is not far from the actual behaviour.

It can be noticed from figure 7 that the deformation at each material point increases stepwise through the SPIF process. However, within each contour the deformation mode is actually not monotonic and strain path changes take place. This phenomenon is more obvious if we present the whole deformation evolution in the way as shown in figure 9a, where only the radial and circumferential plastic strain are presented. In this figure, the strain components of another element (Element 3' in figure 3) located at the same position as Element 3 but at the outer side of the cone are also illustrated. Apparently the deformation shows a zigzag pattern which corresponds to the movement of the tool towards the material point, passing it and finally moving away. Furthermore, the behavior of the materials through the thickness is non-homogeneous during the process. Figure 9b shows the deformation evolution within one particular contour, for example, the 37th contour. t_1 and t_4 are the starting and ending moment of the deformation within the contour, respectively. This means that at time t_4 the deformation at this material point stops for this contour while the tool continues to move further away from that point. The deformation will start again in the next contour when the tool moves towards the point. t_2 and t_3 are the moments the strain path changes take place. First, it is obvious that the strain level at the outer side is higher than that at the inner side up to this contour, although at the end of the process the deformation through the thickness reaches almost the same value. Secondly, it is clear that within the contour, there is always elongation in the radial direction and thinning in the thickness direction. In the cicumferential direction, for the material close to the inner surface, it is first elongation from t_1 to t_2 and then changes to compression from t_2 to t_3 and finally elongation again from t_3 to t_4,, whereas, for the material at the outer side, the deformation is first compression and then elongation before it changes to compression again, which is just opposite to that at the inner side. This means that the material at a certain point undergoes a deformation of elongation in the radial, thinning in the thickness direction and a kind of bending and unbending in the circumferential direction while the tool passes by. The strain path changes within one contour lead to the accumulation of the deformation and they are repeated contour by contour until the tool is far away from that point. The deformation then reaches the maximum. As a result, the accumulated von Mises equivalent plastic strain is not the same as the apparent one derived directly from the strain components. The accumulated and apparent von Mises equivalent plastic strain can be calculated respectively by equation (2), and (3):

$$\bar{e}_{vm}^{acc} = \int_0^t \dot{e}_{vm} dt \quad \text{with} \quad \dot{e}_{vm} = \sqrt{\frac{2}{3}\dot{e}_{ij}^{pl}\dot{e}_{ij}^{pl}} \tag{2}$$

$$\bar{e}_{vm}^{app} = \sqrt{\frac{2}{3}e_{ij}^{pl}e_{ij}^{pl}} \tag{3}$$

where $\dot{e}_{vm}$ is the von Mises equivalent plastic strain rate, $\dot{e}_{ij}^{pl}$ the components of the plastic strain rate tensor and e_{ij}^{pl} the components of the plastic strain tensor. The accumulated von Mises equivalent plastic strain of one material point is much higher than the apparent one. Figure 10

shows both predicted equivalent strains for different wall angles. The difference between these two equivalent strains depends on the process parameters such as tool diameter and vertical step size. The strain path changes and the resulting accumulated equivalent strain could influence the work hardening behavior of the material during the SPIF process, which should be taken into account during the simulation. The bending and unbending behavior reminds in a lower level the strains imposed by a draw bead in classical deep drawing process. Their effect on material behavior is far from being negligible.

5. Conclusions

This paper investigates the process of single point incremental forming of a cone using the finite element method. By simplifying the numerical model, it is possible to simulate the process so that a better understanding of the deformation mechanism is achieved. Predicted results show good agreement with experimental data for the geometry of the cone. Localised thinning is observed at a high wall angle and can be well predicted. According to the simulation results, the material follows a deformation mode of elongation in the cone radial direction, compression in the thickness direction and a kind of bending and unbending behavior in the circumferential direction. Strain path changes take place during the SPIF process, which do have a significant influence on the material behavior, as will be reported in a forthcoming paper.

Acknowledgement

The authors would like to acknowledge financial support from the Institute for the Promotion of Innovation by Science and Technology in Flanders (IWT). A. Van Bael thanks the Belgian Science Policy for financial support through Contract P5/08. A. M. Habraken is mandated by the National Fund for Scientific Research (Belgium).

References

[1] J. Jeswiet, E. Hagan, Rapid prototyping of a headlight with sheet metal, Proceedings of 9th International Conference on Sheet Metal, Leuven (2001), p165

[2] M. Bambach, G. Hirt, S. Junk, Modelling and experimental evaluation of the incremental CNC sheet metal forming Process, Proceedings of VII International Conference on Computational Plasticity, Barcelona (2003)

[3] S. Matsubara, Incremental backward forming of a sheet metal with a hemispherical head tool- a study of a numerical control forming system, J. of JSTP Vol. 35 (2004), p1311-1316

[4] J. Jeswiet, J. R. Duflou, A. Szekeres, P. Levebre, Custom Manufacture of a Solar Cooker- A Case Study, Advanced Materials Research Vols. 6-8 (2005), p487-492

[5] M. S. Shim, J.J. Park, The formability of aluminium sheet in incremental forming, Journal of Materials Processing Technology 113 (2001), p654-658

[6] E. Hagan, J. Jeswiet, Effect of wall angle on Al3003 strain hardening for parts formed by CNC incremental forming, IMECHE Part B, J. of Engineering Manufacture Vol. 217 (2003), p1571-1581

[7] L. Fratini, G. Ambrogio, R. Di Lorenzo, L. Filice and F. Micari, Influence of mechanical properties of the sheet material on formability in single point incremental forming, CIRP Annals 2004 Vol. 53/1, p207-210

[8] H. Iseki, An approximate deformation analysis and FEM analysis for the incremental bulging of sheet metal using a spherical roller, Journal of Materials Processing Technology 111 (2001), p150-154

[9] G. Hirt, J. Ames, M. Bambach and R. Kopp, Forming Strategies and Process Modelling for CNC Incremental Sheet Forming, CIRP Annals 2004 Vol. 53/1, p. 203-206

[10] M. Bambach, G. Hirt and J. Ames, Modeling of optimization strategies in the incremental CNC sheet metal forming process, Proceedings of the 8th International Conference on Numerical Methods in Industrial Forming Processes, Columbus (2004), p.1969-1974

[11] G. Ambrogio, L. Filice, L. Fratini and F. Micari, Process Mechanics Analysis in Single Point Incremental Forming, Proceedings of the 8th International Conference on Numerical Methods in Industrial Forming Processes, Columbus (2004), p. 922-927

[12] S. He, A. Van Bael, P. Van Houtte, A. Szekeres, J. Duflou, C. Henrard and A.M. Habraken, Finite Element Modeling of Incremental Forming of Aluminium Sheets, Advanced Materials Research Vols. 6-8 (2005), p525-532

[13] C. Henrard, A.M. Habraken, A. Szekeres, J.R. Duflou, S. He, A. Van Bert and P. Van Houtte, Comparison of FEM Simulations for the Incremental Forming Process, Advanced Materials Research Vols. 6-8 (2005), p533-542

[14] Abaqus User´s Manual, version 6.4, 2003

[15] J. Brown, Advanced machining technology handbook, McGraw Hill 1998.

[16] D. Young, J. Jeswiet, Wall thickness variations in single point incremental forming, IMECHE Part B, J. of Engineering Manufacture Vol. 218 (2004), p1-7

[17] T. J. Kim, D. Y. Yang, Improvement of formability for the incremental sheet metal forming process, Int. J. of Mechanical Sciences Vol. 42 (2001), p1271-1286

Figure 1. Exploded view of forming fixture with a formed cone

Figure 2. Diagram of tool path from a side view

Figure 3. Initial and deformed mesh (E1 to E4: element 1 to element 4 in the inner surface layer from the blank outer edge towards the center; E3' same position as E3 but in the outer surface layer)

Figure 4. Inner surfaces of the formed cones with different wall angles

Figure 5. Thickness profiles of deformed cones with different wall angles (the open triangles, diamonds and circles show the experimental results for the wall angles 50°, 60° and 65°, respectively; the lines are the simulation results)

Figure 6. Deformation history during the SPIF process of a 50-degree cone (E1 to E4: elements shown in figure 3)

Figure 7. The evolution of three normal plastic strain components in an element at the inner side of a 50-degree cone (Element 3 in figure 3) during the SPIF process

Figure 8. Coordinate systems defined in the FE model (OXYZ: The fixed global coordinate system with OX parallel to the 0-degree section of the initial sheet mesh and OZ normal to the initial sheet surface. $O_1X_1Y_1Z_1$: A co-rotated local coordinate system assigned to a material point with O_1X_1 parallel to the cone radial direction at that point and O_1Z_1 normal to the sheet.)

Figure 9. The evolution of radial and circumferential plastic strain in elements at the inner (Element 3 in figure 3) and outer side (Element 3') of a 50-degree cone during the SPIF process: (a) during the whole process; (b) within the 37^{th} contour (t_1 and t_4 are the moments the deformation starts and stops within this contour; t_2 and t_3 are the moments the strain path changes take place)

Figure 10. Predicted maximum von Mises equivalent plastic strains for different wall angles

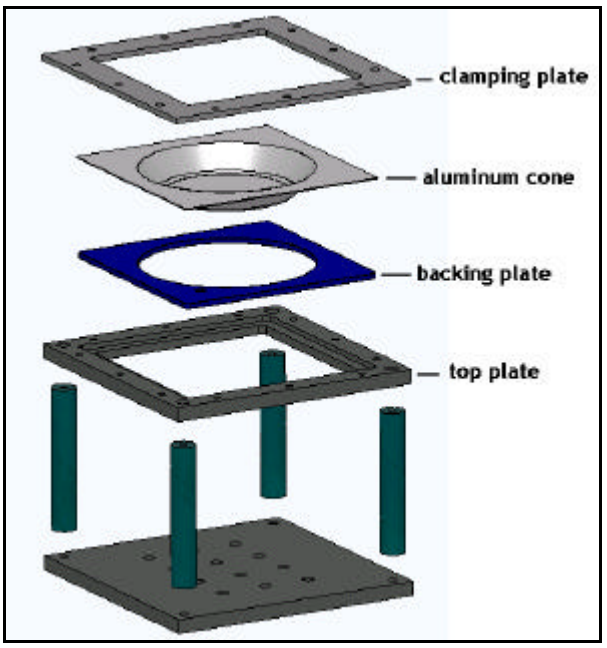

Figure 1

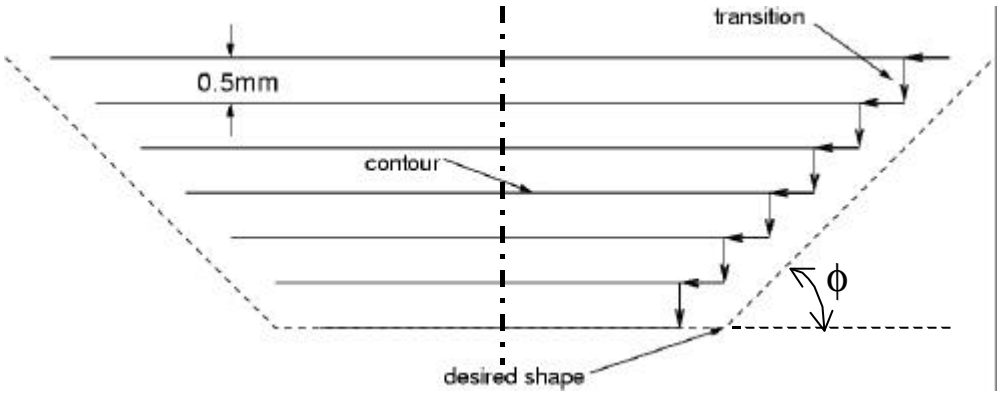

Figure 2

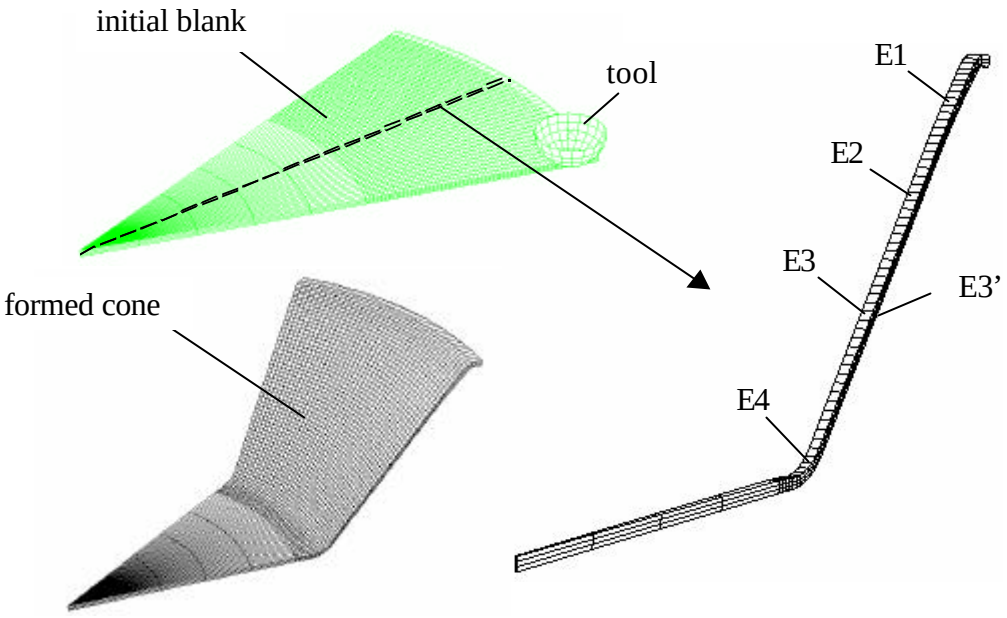

Figure 3

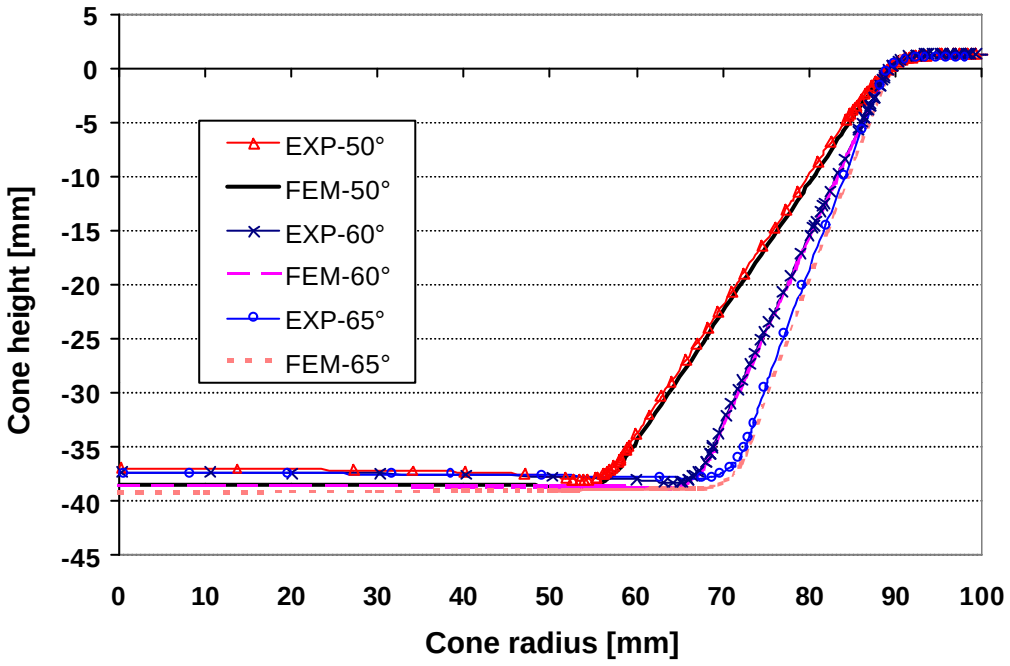

Figure 4

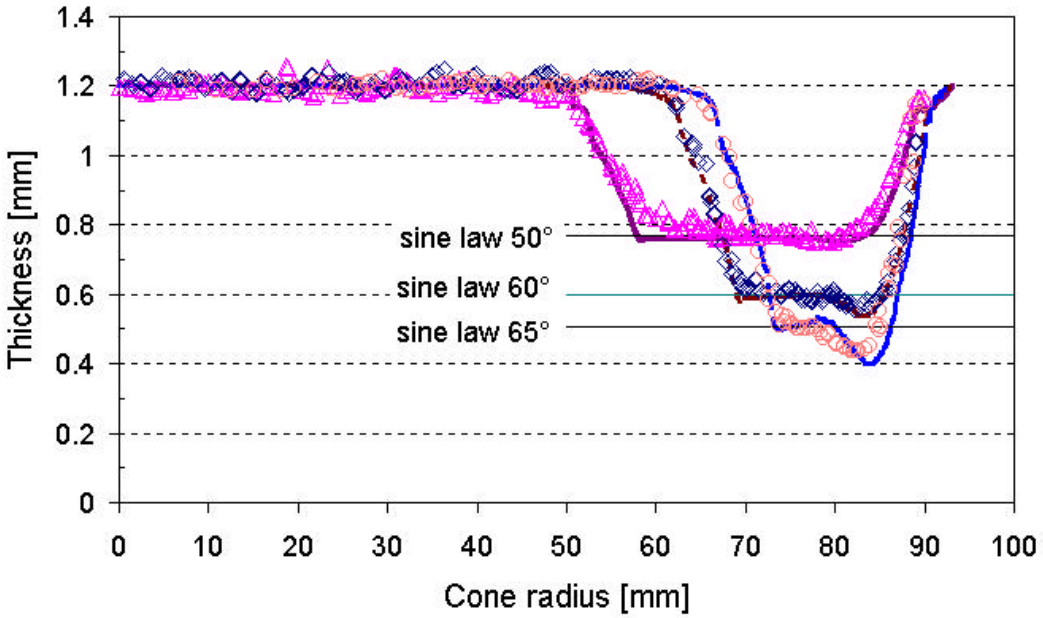

Figure 5

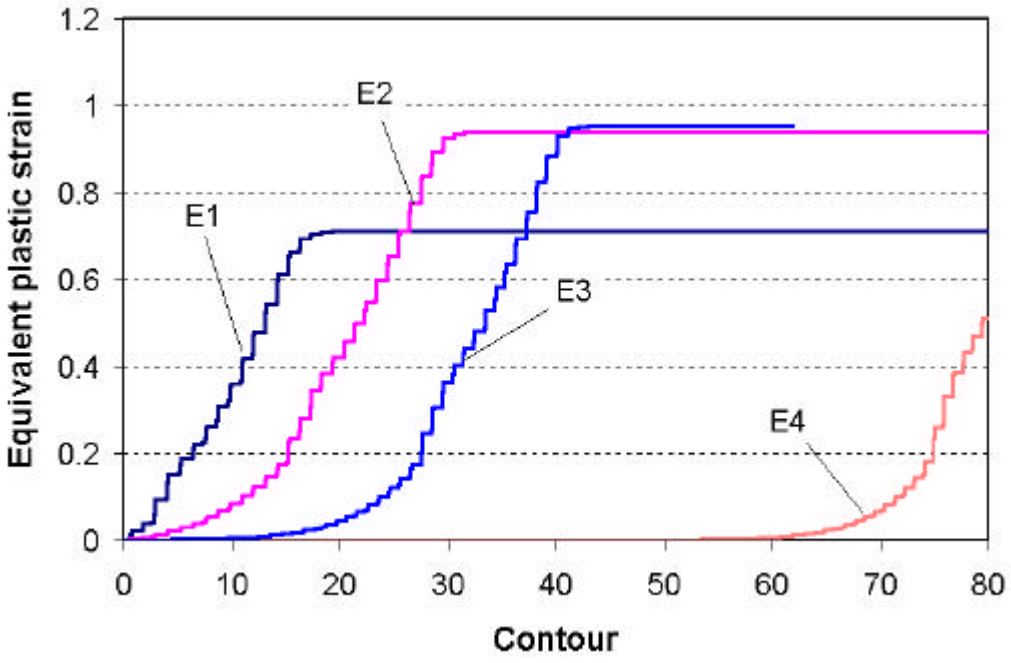

Figure 6

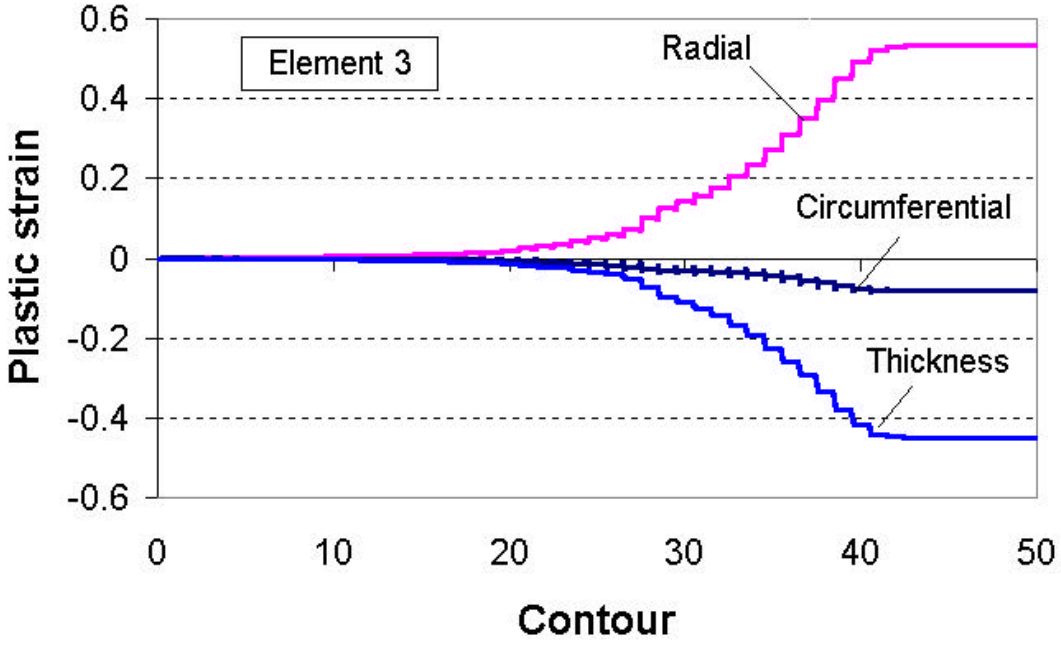

Figure 7

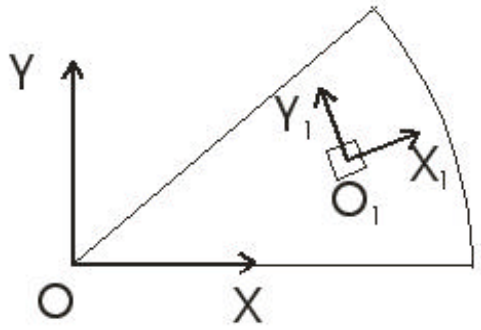

Figure 8

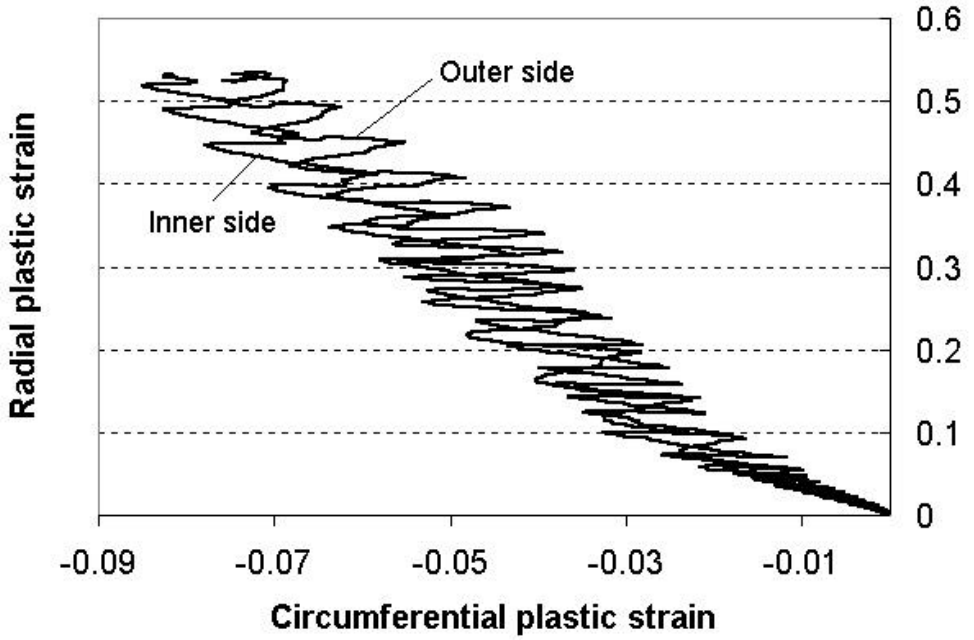

Figure 9 (a)

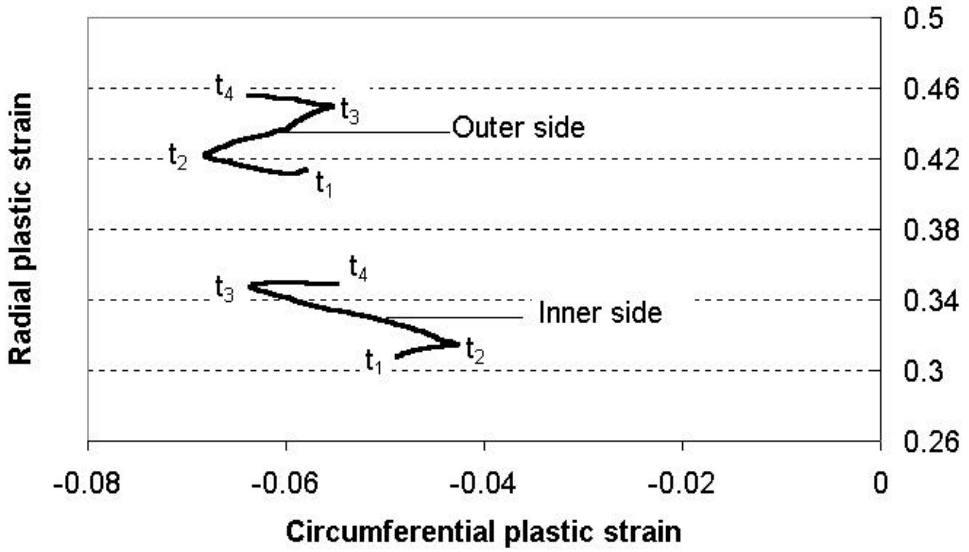

Figure 9 (b)

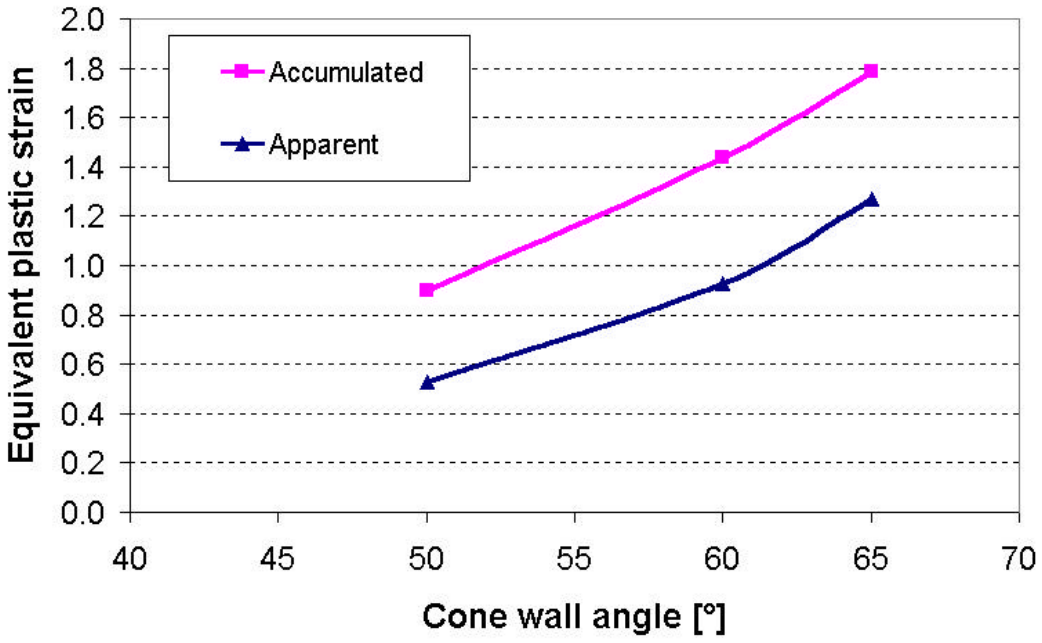
Equivalent plastic strain
2.0
1.8
1.6
1.4
1.2
1.0
0.8
0.6
0.4
0.2
0.0
Accumulated
Apparent
40
45
50
55
60
65
70
Cone wall angle [°]

Figure 10